

Rapid neutron star equation of state inference with Normalising Flows

Jordan McGinn,¹ Arunava Mukherjee,^{2,1,*} Jessica Irwin,^{1,†}
Christopher Messenger,¹ Michael J. Williams,¹ and Ik Siong Heng¹

¹*SUPA, School of Physics and Astronomy, University of Glasgow, Glasgow G12 8QQ, United Kingdom*

²*Saha Institute of Nuclear Physics, A CI of HBNI, 1/AF Bidhannagar, Kolkata-700064, India*

(Dated: March 27, 2024)

The first direct detection of gravitational waves from binary neutron stars on the 17th of August, 2017, (GW170817) heralded the arrival of a new messenger for probing neutron star astrophysics and provided the first constraints on neutron star equation of state from gravitational wave observations. Significant computational effort was expended to obtain these first results and therefore, as observations of binary neutron star coalescence become more routine in the coming observing runs, there is a need to improve the analysis speed and flexibility. Here, we present a rapid approach for inferring the neutron star equation of state based on Normalising Flows. As a demonstration, using the same input data, our approach, **ASTREOS**, produces results consistent with those presented by the LIGO-Virgo collaboration but requires < 1 sec to generate neutron star equation of state confidence intervals. Furthermore, **ASTREOS** allows for non-parametric equation of state inference. This rapid analysis will not only facilitate neutron star equation of state studies but can potentially enhance future alerts for electromagnetic follow-up observations of binary neutron star mergers.

Introduction.— On 17 August 2017, during the second advanced detector observing run, advanced LIGO [1] and advanced Virgo [2] observatories detected the first gravitational wave (GW) signal from the coalescence of two neutron stars (NSs) [3, 4]. The global network made a second GW observation consistent with a signal from a binary neutron star (BNS) collision [5] during the 3rd observing run. In addition, two other GW events likely originating from the mergers between pairs of NSs and black holes were reported [6]. To date, there have been more than 90 definitive GW event detections, with the vast majority being the merger of binary black holes (BBHs) [7]. However, for merging systems containing one or more NSs the presence of matter requires that tidal effects be taken into account when modelling the inspiral stage of the waveform. It is the tidal deformation that each star’s gravitational field induces on its companion that accelerates the decay of the inspiraling orbit and imprints itself on the emitted GW signals. These detections therefore provide a new opportunity to probe matter in extreme conditions [8] present in the interior of these stars, now confirmed through observation [3, 9].

NSs are the densest observable objects in the universe where densities at the centre of the star can reach about ~ 6 – 8 times the saturation density (ρ_0) [10, 11]. Properties of hadronic matter at such a high density and low temperature have not been probed by any experiment or observation except those targeting NSs. A NS’s tidal deformability parameter (Λ) along with its mass (m), provides information on its interior composition via the underlying equation of state (EOS) [12–14]. Thus, astrophysical inference of m and Λ of a NS can provide useful constraints on the NS EOS. This in turn provides valuable insights into the nature of nuclear interactions of

hadronic matter, which are governed by strong nuclear interactions at high density/chemical potentials in degenerate conditions [15]. Each theoretical model for this nuclear interaction provides a different EOS, i.e., density (ρ) vs pressure (P) relationship.

The EOS is assumed to be universal for all NSs in the sense that there is a single relationship between P and ρ common for all such stars. Each star is free to have its own independent mass m and associated tidal deformability Λ , governed by the underlying EOS. A fully Bayesian approach [16] showed that detections of $\mathcal{O}(10)$ BNS mergers in the advanced detector era could constrain the EOS significantly. This work was expanded when [17] used Markov chain Monte Carlo simulations of the $P(\rho)$ relationships under a piece-wise polytropic parametrisation of the EOS [18]. The first detection of BNS event [3] has allowed constraints to be placed on the $m - \Lambda$ parameter plane. Follow-up analysis of the GW170817 event has been able to further constrain the EOS [9, 19]. Subsequently, several Bayesian analyses have been performed to simulate inference for multiple BNS events [20–23].

The LIGO and Virgo collaborations applied two different methods of analysis to inferring the EOS of the BNS merger GW170817 [9]. In one method, both components of the merger were assumed to be governed by the same EOS, represented by a spectral parametrisation to describe their collective $P(\rho)$ relationship [24]. The second method is regarded as EOS-insensitive but retains the assumption that both NSs are governed by the same EOS. Macroscopic properties of the NSs are related to derive an expression for the asymmetric tidal deformability of the components in a binary system. The relationships established depend loosely on the EOS and are tuned to a wide variety of possible EOS models, such that the individual tidal deformability pairs recovered can map to the correct waveform template, independent of EOS model [25]. Recently, there has been some effort to incorporate non-

* arunava.mukherjee@saha.ac.in

† j.irwin.1@research.gla.ac.uk

parameteric inference of models using Gaussian processes conditioned on realistic NS EOSs [26, 27].

The success of traditional Bayesian sampling techniques when applied to NS EOS inference depends not only on the observed GW signals but also on the choice of parametrization. The simplest and most widely used form of the NS EOS is the piecewise polytropic model [18]. However, this representation is not unique, and it does not ensure causality of sound speed for NS matter. Moreover, applying traditional Bayesian sampling techniques causes undesirable sampling issues [28] around the transition densities of different polytropic regions [17]. The spectral representation [29, 30] provides us with a better parameterization of the EOS that ensures both thermodynamic stability and causality conditions. However, an implementation of spectral parameterization for Bayesian sampling is computationally expensive and cumbersome. Furthermore, it quickly becomes quite complex, for example, to implement density-dependent constraints on the EOS parameter space corresponding to different terrestrial nuclear physics experiments at lower densities, along with astronomical observations at the medium density regime, and model agnostic and non-parametric aspects of the higher density part [11, 31] of the EOS.

Thus, the existing traditional Bayesian sampling methods have a major limitation in performing statistical inference from different families of models corresponding to different sets (and also different numbers) of parameters. This is in addition to the fact that such techniques can also be extremely computationally expensive. The issue of analysis latency is further compounded by the significant increase in the number of BNS detections expected as the sensitivities of advanced detectors improve [32]. To perform EOS inference on BNS merger events during future GW advanced detector observing runs, rapid inference tools are needed to act upon event data at low latency that can be easily combined with other standard low-latency pipelines.

Recent advances in machine learning (ML) have been successfully applied to GW data analysis [33]. These include parameter estimation [34–39], waveform modelling [40, 41] and searches [42–44]. One clear motivation behind using ML to either supplement or replace existing algorithms is that, once trained, the ML algorithm can run using a significantly lower fraction of the computational cost and time. ML algorithms are also naturally more flexible and can account for hard-to-model or unmodelled components of the analysis.

In this letter, we describe an ML approach to provide posterior distributions describing the NS EOS. As input we use the standard parameter estimation data products (posterior samples) on the gravitational masses (m) and the tidal deformabilities (Λ) of the components within a BNS system. Such data are generated as a standard output product as part of the data release associated with detected BNS events [45]. The output of our normalising flow (NF) [46, 47] based analysis is an en-

semble of non-parametric EOSs describing the relationship between pressure and energy density within NSs. In addition, we output correlated samples of NS central densities and maximum permitted densities corresponding to its TOV-limit. Hence, once trained, the NF acts as a rapid functional generator of plausible NS EOSs.

Method.— A NF is a generative ML model that learns to transform samples from a given distribution to a simpler “latent” distribution via a series of invertible mappings. One advantage NFs have over other generative models (Generative Adversarial Networks [48], Variational Auto-Encoders [49]) is that they learn the probability density function of the training data explicitly. At the training stage, a conditional NF learns to map samples x in the data space \mathcal{X} and y in the conditional data space \mathcal{Y} to a point z in latent space \mathcal{Z} such that the following function holds:

$$p_{\mathcal{X}|\mathcal{Y}}(x|y) = p_{\mathcal{Z}}(f(x|y)) \left| \det \left(\frac{\partial f(x|y)}{\partial x} \right) \right|, \quad (1)$$

where f is the bijective mapping $f : \mathcal{X} \rightarrow \mathcal{Z}$ and $\partial f(x|y)/\partial x$ is the Jacobian of f evaluated at x . This requires transforms whose Jacobian determinants are tractable and easy to compute. In this work we use a real non-volume preserving (Real NVP) NF [50] which uses stacked *coupling transforms*. As the learned transforms are invertible, samples can be drawn from $p_{\mathcal{X}|\mathcal{Y}}$ by sampling from $p_{\mathcal{Z}}$ and applying the inverse transform f^{-1} . (For further details on NFs, please see [46, 47].)

Our aim is to use a conditional NF to accurately approximate a function that maps values of the component masses and tidal deformabilities of a BNS system, $y = (m_1, m_2, \Lambda_1, \Lambda_2)$, to an associated set of EOS information x , parameterised for convenience by a principle component analysis (PCA) decomposition (see IA for details), the central densities of each star ρ_c , and a maximally allowed central density ρ_{\max} for the EOS in question. We refer to these latter three quantities as *auxiliary parameters* and we call our analysis **ASTREOS**.

Our training data consists of 10^5 phenomenological NS EOSs represented initially as energy-density computed on a fixed vector of pressure values. This is compressed into a lower-dimensional representation using PCA and accompanied by the maximum allowed energy density ρ_{\max} for each EOS - this and the auxiliary parameters define the data space \mathcal{X} . To associate each x to a corresponding GW observable y we first sample from a uniform prior on the joint mass distribution with fixed lower bound $0.5M_{\odot}$, an upper bound dictated by the EOS and ρ_{\max} , and the constraint $m_1 \geq m_2$. These choices then define the value of tidal deformability for each NS in the binary as well as the central energy-density of each component.

We use an implementation of NFs called **GLASFLOW** [51] based on **NFLOWS** [52] which is written for **PYTORCH** [53]. Our present version is implemented by a modification of an initial network outlined in [54]. We train the flow for 5000 epochs with a batch size of 4096 and initial learn-

ing rate of 0.005 which is decayed to zero using cosine annealing [55] together with the AdamW [56] optimiser. There are two residual blocks for each of the three coupling transforms which each contain 151 neurons. We use Batch Normalisation between each coupling transform [50] and optimise hyper-parameters using “Weights & Biases” [57]. Data is split between 80% training and 20% validation and on a NVIDIA Tesla V100 (or equivalent) training requires $\mathcal{O}(3)$ hours with a GPU memory footprint of ~ 2 GB.

The NF allows us to model the distribution $p_{\mathcal{X}|Y}(x|y)$ but our knowledge of y for a given BNS event is limited to the posterior $p(y|h)$ given the observed strain h . Therefore we must marginalise over the correlated uncertainties in y due to the GW detector noise and other correlations between these and other GW parameters. Our final inference on the EOS and auxiliary parameters for a given BNS observation is given by

$$p(x|h) = \int p_{\mathcal{X}|Y}(x|y)p(y|h) dy \quad (2)$$

where, rather than evaluating this integral directly, samples from $p(x|h)$ are obtained by drawing an equal number of samples (usually one) from $p_{\mathcal{X}|Y}(x|y_j)$ for each posterior sample y_j .

Results.— We demonstrate the effectiveness of our model by analysing the GW170817 event using posterior samples [58] associated with [59] available from the Gravitational Wave Open Science Center [60]. These samples do not assume any inherent correlation between individual NS tidal deformabilities or that they share the same universal EOS.

To perform EOS inference of GW170817 using ASTREOS, as input we used the joint posterior samples of $m_1, m_2, \Lambda_1, \Lambda_2$ to represent the conditional y component in the NF. These posterior samples were computed assuming low-spin priors on the point-mass parameters, the most relevant of which are the uniform priors on the detector frame component mass with constraints $0.5M_\odot \leq m_2 \leq m_1 \leq 7.7M_\odot$ and uniform priors on component tidal deformabilities $\Lambda_{1,2} \in [0, 5000]$.

In order to use the NF model for testing, we draw one latent space sample from $p_{\mathcal{Z}}$ for each posterior sample y_j from the GW170817 posterior $p(y|h)$ and apply the NF mapping to obtain a sample x . We discard any posterior samples that lie outside of our prior training space. We repeat the process according to Eq. 2 to build up a distribution of samples from the final EOS posterior $p(x|h)$, discarding any output samples that lie outside our 10-dimensional prior training space [61]. It takes only $\mathcal{O}(0.1)$ sec to generate and convert 2500 posterior samples to correctly normalised EOS curves.

Our main GW170817 result is compared to the spectral parametrisation analysis of [9] in Fig. 1 where we show EOS confidence intervals on energy-density as a function of pressure. We also show cumulative probability curves obtained from ASTREOS for pressure and energy-density for each NS and similar curves for the correspond-

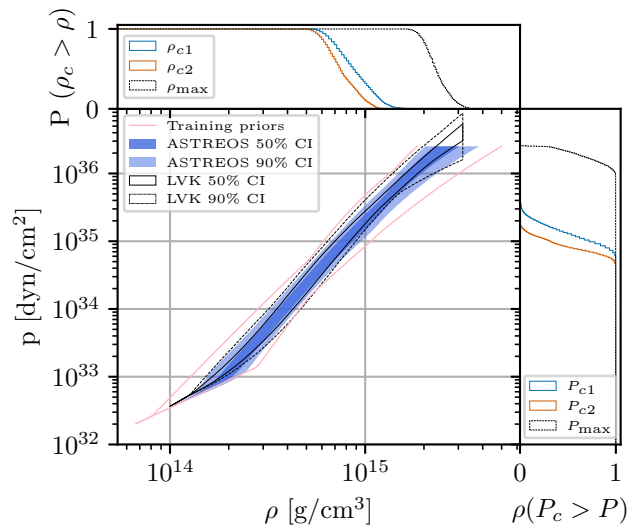


FIG. 1. The pressure p as a function of energy-density ρ for the GW170817 event. We show posteriors on energy density as a function of pressure obtained from ASTREOS (blue bands) together with posteriors taken from GW170817 LIGO-Virgo spectral parameterisation analysis [9] (black lines) and the ASTREOS prior training bounds (pink lines). The dark blue and light blue shaded regions for ASTREOS, and the solid and dashed lines for the LIGO-Virgo analysis, correspond to the symmetric 90% and 50% confidence intervals respectively. The top panel shows the ASTREOS posterior survival functions on the central energy-densities of each star $\rho_{c,1}$, $\rho_{c,2}$ (blue and red), and the maximum energy-density ρ_{\max} (black). The panel on the right shows the same for the pressure quantities $p_{c,1}$, $p_{c,2}$ (blue and red) and p_{\max} (black).

ing maximum allowed pressures and energy-densities of the inferred EOS. We note that a possible reason for the discrepancy between the results towards higher energy densities is the difference between the training prior distribution of EOSs and that assumed for the LIGO-Virgo analysis. Both the LIGO-Virgo spectral parameterisation and the input samples to ASTREOS use priors uniform in component mass. We can also rule out the choice of the lower component mass prior boundary used in training the NF (since they are identical) and although the upper bounds do differ (the maximum component mass used in training is $3M_\odot$) we retain only GW170817 samples lie within the training space.

To further verify the statistical consistency of the ASTREOS analysis, we provide a probability-probability (p-p) plot [62, 63] in Fig. 2 with curves for each of the output EOS and auxiliary parameters. It shows the fraction of true parameter values that lie within a given confidence interval as a function of confidence interval. Curves that trace the diagonal within the uncertainty bounds dictated by the number of simulated cases, indicate statistical consistency of the inferred parameter distributions output from the NF. This result represents an isolated test of the statistical robustness of the ASTREOS analysis

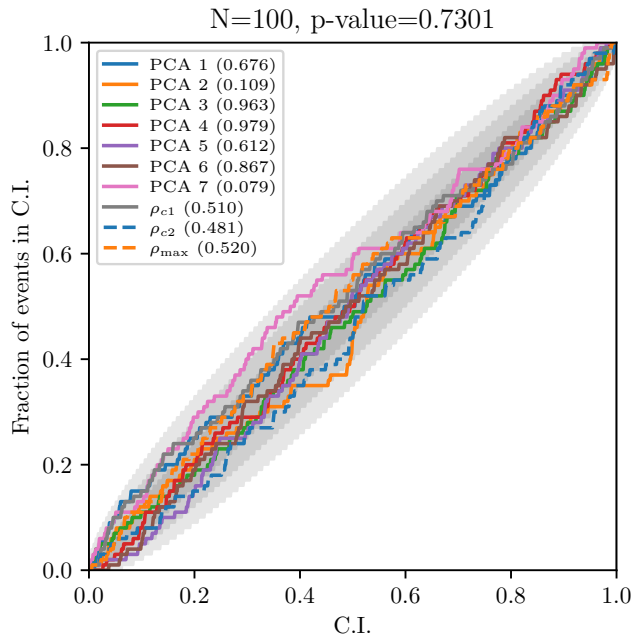


FIG. 2. A p-p plot on the 10 inferred EOS and auxiliary parameters output from the **ASTREOS** analysis using 100 instances of conditional data y drawn from the validation set. The bracketed quantities in the plot legend refer to the p-values of each parameter curve under the null hypothesis that each curve traces the diagonal. The gray error bands represent the 1,2 and 3σ confidence intervals for each curve and the combined parameter p-value for the null hypothesis is 0.7301.

and does not include the use of posterior GW samples $p(y|h)$. The process tests the statistical consistency of the $p(x|y)$ (the NF component) only. In this test we draw single instances of EOS and auxiliary parameters (x) from our validation set together with their associated mass and tidal deformability parameters (y). For the purposes of the p-p test, x then defines the “truth” and y is then input to **ASTREOS** to obtain 2000 samples drawn from the posterior $p(x|y)$. This process is repeated 100 times allowing the construction of the p-p plot shown in Fig. 2 and resulting in a combined p-value of 0.7301. There is no additional marginalisation over the uncertainty on y as would be the case had we simulated samples from $p(y|h)$. This allows us to verify the correctness of the NF unaffected by additional independent components of a full GW analysis pipeline.

Conclusions.— In this Letter we have for the first time demonstrated that neural networks can accurately infer NS EOS curves conditioned on prior measurements of component masses and tidal deformabilities within a strict Bayesian framework. The NF architecture of our analysis learns the distribution of plausible EOSs consistent with the conditional argument and naturally marginalises over the uncertainty inherent to the GW measurement. The analysis also provides estimates of the central energy-densities of both the component NSs

and the maximally allowed energy-density of the EOS.

Once trained, the network can generate ~ 25000 samples per second from the EOS posterior meaning that EOS posteriors can be obtained almost immediately after a GW parameter estimation (PE) analysis has completed. We note that the NF need only be trained once, after which all events can be analysed rapidly. Coupled with the growing number of ultra-low latency ML PE pipelines [34, 36, 39], rapid inference on EOS properties can then be used to inform low-latency Electromagnetic (EM) follow-up observations regarding the likelihood of prompt EM emission.

We would like to stress the model independence of our approach and clarify that although the EOS outputs of our analysis are parameterised via PCA coefficients, the training data can in principle be composed of any EOS model or mixture of models. It is therefore the choice of training data that defines the prior on the EOS parameter space and allows the user to be as constraining, or flexible, as they want. The minimal requirement from any model is that it is possible to sample a component mass and compute the corresponding tidal deformability for a given EOS represented via a vector of pressure as a function of energy-density. We would also note that our analysis can be easily modified to handle neutron star-black hole (NSBH) systems [6, 7] where the conditional data in this case would consist of only one pair of mass and tidal deformability parameters.

As is evident from the GW170817 result presented in Fig. 1, for individual GW events the information content and constraints placed on the prior EOS space is relatively modest. However, the number of additional BNS (and NSBH) expected events [64] in the ongoing O4 observing run of the advanced GW detector network will allow EOS inference results to be combined. With this combination on the universal EOS parameters we would expect an approximate \sqrt{N} reduction [65] in the uncertainty represented in Fig. 1 where N is the number of detections. Fortunately NFs are ideally suited for combining results by making use of the trained Jacobian (see Eq. 1). Instead of generating samples from $p(x|h)$, it is possible to directly evaluate the distribution for each event either on a common grid of x values or through a sampling algorithm, e.g., Markov chain Monte Carlo.

Acknowledgement.— This material is based upon work supported by NSF’s LIGO Laboratory which is a major facility fully funded by the National Science Foundation. The authors would like to thank members of the LIGO-Virgo-Kagra extreme matter group for valuable input, specifically Jocelyn Read, Lami Suleiman, Katerina Chatziioannou, Isaac Legred, Jolien Creighton, and Md. Emanuel Hoque. AM acknowledges support from the DST-SERB Start-up Research Grant SRG/2020/001290 and partial computational support from Newton-Bhabha Grant. AM, CM, ISH acknowledge partial support from Science and Technology Research Council (Grant No. ST/L000946/1). CM is also supported by the European Cooperation in Science and Technology (COST) action

[CA17137].

The authors acknowledge the usage of the analysis soft-

ware NFLOWS [52], GLASFLOW [51], BILBY [66] and open data resource from GWOSC [67].

-
- [1] J. Aasi *et al.* (LIGO Scientific), *Class. Quant. Grav.* **32**, 074001 (2015), [arXiv:1411.4547 \[gr-qc\]](#).
- [2] F. Acernese *et al.* (VIRGO), *Class. Quant. Grav.* **32**, 024001 (2015), [arXiv:1408.3978 \[gr-qc\]](#).
- [3] B. Abbott and *et al.*, *Physical Review Letters* **119**, 10.1103/physrevlett.119.161101 (2017).
- [4] B. P. Abbott, *et al.* LIGO Scientific Collaboration, Virgo Collaboration, and S. South Africa/MeerKAT, *Astrophysical Journal Letters* **848**, L12 (2017), [arXiv:1710.05833 \[astro-ph.HE\]](#).
- [5] B. P. Abbott and *et al.*, *The Astrophysical Journal* **892**, L3 (2020).
- [6] R. Abbott and *et al.*, *The Astrophysical Journal Letters* **915**, L5 (2021).
- [7] The LIGO Scientific Collaboration, the Virgo Collaboration, the KAGRA Collaboration, *et al.*, *arXiv e-prints*, [arXiv:2111.03606 \(2021\)](#), [arXiv:2111.03606 \[gr-qc\]](#).
- [8] J. M. Lattimer and M. Prakash, *Science* **304**, 536 (2004), [arXiv:astro-ph/0405262 \[astro-ph\]](#).
- [9] B. P. Abbott and *et al.* (The LIGO Scientific Collaboration and the Virgo Collaboration), *Phys. Rev. Lett.* **121**, 161101 (2018).
- [10] J. M. Lattimer and M. Prakash, *Phys. Report* **442**, 109 (2007), [arXiv:astro-ph/0612440 \[astro-ph\]](#).
- [11] M. M. Forbes, S. Bose, S. Reddy, D. Zhou, A. Mukherjee, and S. De, *Phys. Rev. D* **100**, 083010 (2019).
- [12] S. De, D. Finstad, J. M. Lattimer, D. A. Brown, E. Berger, and C. M. Biwer, *Phys. Rev. Lett.* **121**, 091102 (2018), [arXiv:1804.08583 \[astro-ph.HE\]](#).
- [13] T. Dietrich, M. W. Coughlin, P. T. H. Pang, M. Bulla, J. Heinzl, L. Issa, I. Tews, and S. Antier, *Science* **370**, 1450 (2020), [arXiv:2002.11355 \[astro-ph.HE\]](#).
- [14] S. M. A. Imam, A. Mukherjee, B. K. Agrawal, and G. Banerjee, *arXiv e-prints*, [arXiv:2305.11007 \(2023\)](#), [arXiv:2305.11007 \[nucl-th\]](#).
- [15] J. M. Lattimer, *Annual Review of Nuclear and Particle Science* **71**, 433 (2021).
- [16] W. Del Pozzo, T. G. F. Li, M. Agathos, C. Van Den Broeck, and S. Vitale, *Phys. Rev. Lett.* **111**, 071101 (2013).
- [17] B. D. Lackey and L. Wade, *Phys. Rev. D* **91**, 043002 (2015).
- [18] J. S. Read, B. D. Lackey, B. J. Owen, and J. L. Friedman, *Phys. Rev. D* **79**, 124032 (2009), [arXiv:0812.2163 \[astro-ph\]](#).
- [19] M. Al-Mamun, A. W. Steiner, J. Nättilä, J. Lange, R. O’Shaughnessy, I. Tews, S. Gandolfi, C. Heinke, and S. Han, *Phys. Rev. Lett.* **126**, 061101 (2021).
- [20] I. Legred, K. Chatziioannou, R. Essick, S. Han, and P. Landry, *Phys. Rev. D* **104**, 063003 (2021).
- [21] S. Huth, P. T. H. Pang, I. Tews, T. Dietrich, A. Le Fèvre, A. Schwenk, W. Trautmann, K. Agarwal, M. Bulla, M. W. Coughlin, and C. Van Den Broeck, *Nature (London)* **606**, 276 (2022), [arXiv:2107.06229 \[nucl-th\]](#).
- [22] J. Golomb and C. Talbot, *The Astrophysical Journal* **926**, 79 (2022).
- [23] A. Ray, M. Camilo, J. Creighton, S. Ghosh, and S. Morisaki, *Phys. Rev. D* **107**, 043035 (2023).
- [24] L. Lindblom, *Phys. Rev. D* **82**, 103011 (2010).
- [25] K. Chatziioannou, C.-J. Haster, and A. Zimmerman, *Phys. Rev. D* **97**, 104036 (2018).
- [26] P. Landry and R. Essick, *Phys. Rev. D* **99**, 084049 (2019), [arXiv:1811.12529 \[gr-qc\]](#).
- [27] R. Essick, P. Landry, and D. E. Holz, *Phys. Rev. D* **101**, 063007 (2020), [arXiv:1910.09740 \[astro-ph.HE\]](#).
- [28] M. F. Carney, L. E. Wade, and B. S. Irwin, *Phys. Rev. D* **98**, 063004 (2018).
- [29] L. Lindblom, *Phys. Rev. D* **82**, 103011 (2010), [arXiv:1009.0738 \[astro-ph.HE\]](#).
- [30] L. Lindblom and N. M. Indik, *Phys. Rev. D* **89**, 064003 (2014), [arXiv:1310.0803 \[astro-ph.HE\]](#).
- [31] N. K. Patra, A. Venneti, S. M. A. Imam, A. Mukherjee, and B. K. Agrawal, *Phys. Rev. C* **107**, 055804 (2023), [arXiv:2302.03906 \[nucl-th\]](#).
- [32] The LIGO Scientific Collaboration, the Virgo Collaboration, *et al.*, *Living Reviews in Relativity* **19**, 1 (2016).
- [33] E. Cuoco and *et al.*, *Mach. Learn.: Sci. Technol.* **2**, 011002 (2020).
- [34] H. Gabbard, C. Messenger, I. S. Heng, F. Tonolini, and R. Murray-Smith, *Nature Physics* **18**, 112 (2022), [arXiv:1909.06296 \[astro-ph.IM\]](#).
- [35] A. J. K. Chua and M. Vallisneri, *Phys. Rev. Lett.* **124**, 041102 (2020).
- [36] S. R. Green and *et al.*, *Phys. Rev. D* **102**, 104057 (2020).
- [37] M. J. Williams and *et al.*, *Phys. Rev. D* **103**, 103006 (2021).
- [38] M. Dax, S. R. Green, J. Gair, J. H. Macke, A. Buonanno, and B. Schölkopf, *Phys. Rev. Lett.* **127**, 241103 (2021), [arXiv:2106.12594 \[gr-qc\]](#).
- [39] M. Dax, S. R. Green, J. Gair, M. Pürrer, J. Wildberger, J. H. Macke, A. Buonanno, and B. Schölkopf, *Phys. Rev. Lett.* **130**, 171403 (2023), [arXiv:2210.05686 \[gr-qc\]](#).
- [40] J. McGinn, C. Messenger, M. J. Williams, and I. S. Heng, *Classical and Quantum Gravity* **38**, 155005 (2021).
- [41] D. Williams, I. S. Heng, J. Gair, J. A. Clark, and B. Khamesra, *Phys. Rev. D* **101**, 063011 (2020).
- [42] D. George and E. A. Huerta, *arXiv e-prints*, [arXiv:1711.07966 \(2017\)](#), [arXiv:1711.07966 \[gr-qc\]](#).
- [43] H. Gabbard, M. Williams, F. Hayes, and C. Messenger, *Phys. Rev. Lett.* **120**, 141103 (2018).
- [44] J. Bayley, C. Messenger, and G. Woan, *Phys. Rev. D* **102**, 083024 (2020).
- [45] <https://dcc.ligo.org/ligo-p2000193/public> (2023).
- [46] I. Kobyzev, S. J. Prince, and M. A. Brubaker, *IEEE Transactions on Pattern Analysis and Machine Intelligence* **43**, 3964–3979 (2021).
- [47] G. Papamakarios, E. Nalisnick, D. J. Rezende, S. Mohamed, and B. Lakshminarayanan, Normalizing flows for probabilistic modeling and inference (2021), [arXiv:1912.02762 \[stat.ML\]](#).
- [48] I. Goodfellow, J. Pouget-Abadie, M. Mirza, B. Xu, D. Warde-Farley, S. Ozair, A. Courville, and Y. Bengio, in *Advances in Neural Information Processing Systems*, Vol. 27, edited by Z. Ghahramani, M. Welling, C. Cortes,

- N. Lawrence, and K. Q. Weinberger (Curran Associates, Inc., 2014).
- [49] D. P. Kingma and M. Welling, Auto-encoding variational bayes (2014), [arXiv:1312.6114 \[stat.ML\]](#).
- [50] L. Dinh, J. Sohl-Dickstein, and S. Bengio, Density estimation using real nvp (2017), [arXiv:1605.08803 \[cs.LG\]](#).
- [51] M. J. Williams, jmcginn, federicostak, and J. Veitch, [uof-gravity/glasflow: v0.2.0](#) (2023).
- [52] C. Durkan, A. Bekasov, I. Murray, and G. Papamakarios, [nflows: normalizing flows in PyTorch](#) (2020).
- [53] A. Paszke, S. Gross, F. Massa, A. Lerer, J. Bradbury, G. Chanan, T. Killeen, Z. Lin, N. Gimelshein, L. Antiga, A. Desmaison, A. Kopf, E. Yang, Z. DeVito, M. Raison, A. Tejani, S. Chilamkurthy, B. Steiner, L. Fang, J. Bai, and S. Chintala, in *Advances in Neural Information Processing Systems 32* (Curran Associates, Inc., 2019) pp. 8024–8035.
- [54] J. McGinn, A. Mukherjee, C. Messenger, M. Williams, and I. S. Heng, [Rapid neutron star equation of state inference with normalising flows](#) (2022).
- [55] I. Loshchilov and F. Hutter, [Sgdr: Stochastic gradient descent with warm restarts](#) (2016).
- [56] I. Loshchilov and F. Hutter, [arXiv e-prints](#) , [arXiv:1711.05101 \(2017\)](#), [arXiv:1711.05101 \[cs.LG\]](#).
- [57] L. Biewald, [Experiment tracking with weights and biases](#) (2020), software available from wandb.com.
- [58] <https://dcc.ligo.org/LIGO-P1800370/public>.
- [59] The LIGO Scientific Collaboration, the Virgo Collaboration, *et al.*, *Physical Review X* **9**, 031040 (2019), [arXiv:1811.12907 \[astro-ph.HE\]](#).
- [60] [Gravitational wave open science center \(gwosc\)](#) (2022).
- [61] We use a combination of Convex Hull modelling and a Gaussian mixture model of the prior to perform sample rejection for the conditional y and EOS x space respectively.
- [62] S. R. Cook, A. Gelman, and D. B. Rubin, *Journal of Computational and Graphical Statistics* **15**, 675 (2006), <https://doi.org/10.1198/106186006X136976>.
- [63] S. Talts, M. Betancourt, D. Simpson, A. Vehtari, and A. Gelman, [arXiv e-prints](#) , [arXiv:1804.06788 \(2018\)](#), [arXiv:1804.06788 \[stat.ME\]](#).
- [64] The LIGO Scientific Collaboration, the Virgo Collaboration, the KAGRA Collaboration, *et al.*, *Living Reviews in Relativity* **21**, 3 (2018), [arXiv:1304.0670 \[gr-qc\]](#).
- [65] This rough scaling behaviour is only really true for large N where the variation in individual event signal-to-noise ratio is averaged over. GW170817 was a relatively loud event and hence the initial trend with increasing detections is likely to be less powerful than the \sqrt{N} relation.
- [66] G. Ashton, M. Hübner, P. D. Lasky, C. Talbot, K. Ackley, S. Biscoveanu, Q. Chu, A. Divakarla, P. J. Easter, B. Goncharov, F. H. Vivanco, J. Harms, M. E. Lower, G. D. Meadors, D. Melchor, E. Payne, M. D. Pitkin, J. Powell, N. Sarin, R. J. E. Smith, and E. Thrane, *The Astrophysical Journal Supplement Series* **241**, 27 (2019).
- [67] R. Abbott and LIGO Scientific Collaboration, *SoftwareX* **13**, 100658 (2021), [arXiv:1912.11716 \[gr-qc\]](#).
- [68] I. Jolliffe, *Principal component analysis* (Springer Verlag, New York, 2002).
- [69] E. Chabanat, P. Bonche, P. Haensel, J. Meyer, and R. Schaeffer, *Nuclear Physics A* **635**, 231 (1998).

I. SUPPLEMENTAL MATERIAL

A. Pre-processing and data-preparation for training

Within our training set, each EOS consists of energy density pre-computed on a fixed grid of 256 pressure values which is then truncated to include the 105 grid points spanning the pressure range from 2.024×10^{32} dyn/cm² to 2.517×10^{36} dyn/cm². This preprocessing step is motivated by the necessity to learn only the high density regions of the EOS parameter space where the prior is not already well constrained. For each EOS there exists a different range of possible neutron star masses. We define a uniform prior on this range with a lower bound of $0.5M_{\odot}$ for all EOSs up to the maximum possible mass allowed by each EOS.

We note that although this is a specific choice of component mass prior it does not directly influence the output of our NF. As is clear from Eqs. 1 & 2, the posterior probability on the EOS and auxiliary parameters (x) modelled by the Flow is conditional on the masses and tidal deformabilities (y). The distribution of y is determined solely by the GW posterior $p(y|h)$ (where specific and potentially influential mass and tidal deformability priors have already been applied) and not influenced by their prior distribution during training. The only practical consequence of the choice of training prior is that we should not trust the NF to be well behaved when used on mass and tidal deformability values outside the prior training boundaries. Assuming that these boundaries are well motivated, we can therefore discard any violating input samples from the GW posterior $p(y|h)$ before an analysis.

When selecting training data samples for input to the NF we choose the EOS uniformly from the 10^5 training data examples. This then defines the component mass prior range allowing us to sample the component masses m_1 and m_2 whilst ensuring that $m_1 \geq m_2$. The EOS and masses then naturally determine the central densities of each star in the binary, the tidal deformabilities, and the maximum density allowed by the EOS. With this scheme, it is possible to reuse each of the training EOSs to augment our training data with different choices of component mass. This would allow the Flow to see examples of different binary configurations for repeated EOSs and therefore help the model to generalise over the training prior.

In order to reduce the dimensionality of the problem, ensuring stable and fast training, and to provide a general compression scheme applicable to all EOS model choices, we use a PCA representation [68] of the density as a function of pressure. We choose to represent the EOS data using 7 PCA components (accounting for 99.975% of the variation in the prior training set). All of our training EOS data can therefore be represented with high fidelity using a linear combination of our 7 principle eigenvectors (each of length 105 samples). The data space \mathcal{X} is

therefore reduced to a total of 10 dimensions (7 PCA components plus the 3 auxiliary parameters). As a final preprocessing step, EOS, auxiliary, and conditional parameters are standardised separately by subtracting the mean and scaling to have unit variance. Further, to account for the large dynamic range of the tidal deformability values and central and maximum densities, they are represented by their natural logarithms before standardisation and input to training.

B. Equation of State data used for training the network

We simulate 10^5 phenomenological neutron star EOSs to train the Flow model. To accommodate the analysis within limited computational resources, we generated the EOSs from a 3-piece polytropic neutron star EOS-family widely used in the literature [18]. Each EOS contains a low-density crust described by the SLy4 EOS [69] but at higher densities behaves as a piece-wise polytrope with transition densities at 5×10^{14} g/cm³ and 10^{15} g/cm³. We empirically choose the polytropic indices and their distributions in such a way that the variation in our EOS training set closely follows the prior data-set used in [3]. As we discuss in the conclusions, our method allows for flexibility in the choice of prior EOS model, its parameterisation, and the prior distribution of its parameters. We remind the reader that in any Bayesian analysis the final posterior will to some degree be influenced by the choice of prior.

C. Technical detail about the training method

The training of **ASTREOS** and indeed most NFs involves the process of learning a forward mapping from the training data (the EOS and auxiliary parameters) conditional on labels (the NS component masses and tidal deformabilities) to a zero-mean unit-variance uncorrelated multi-dimensional Gaussian with total dimension equalling that of the training data. Training is performed with the goal of minimising the KL divergence between the learned distribution $p_{\mathcal{X}|Y}(x|y)$ and the distribution of samples in the data space \mathcal{X} . Once trained, we can use **ASTREOS** to perform the inverse mapping from a single condition label y and a randomly drawn location z from the latent space distribution, to an EOS and corresponding auxiliary values x . As we can continually draw random points from the latent space to produce EOS data using the same conditional labels, there will naturally be variation in the output EOS data. This is encoded in the Flow output distribution $p_{\mathcal{X}|Y}(x|y)$. The variation within this distribution is representative of the degeneracy inherent within EOS inference based on single estimates of pairs of component masses and tidal deformabilities. A single value of y maps to a distribution of plausible EOSs all consistent with the input conditional

data and the prior distribution represented by the training data. We repeat this process over a set of mass and tidal deformability samples drawn from the joint posterior $p(y|h)$, where h is the GW strain data for a particular BNS event. By doing this we are able to marginalise over the correlated uncertainties in y due to the GW detector noise and other correlations between these and other GW parameters via Eq. 2.